Clim Dyn
DOI 10.1007/s00382-016-3114-7

Climatology of observed rainfall in Southeast France at the Regional Climate Model scales

Stéphanie Froidurot[1] · Gilles Molinié[1] · Arona Diedhiou[1]

Received: 15 July 2015 / Accepted: 26 March 2016

Abstract In order to provide convenient data to assess rainfall simulated by Regional Climate Models, a spatial database (hereafter called K-REF) has been designed. This database is used to examine climatological features of rainfall in Southeast France, a study region characterized by two mountain ranges of comparable altitude (the Cévennes and the Alps foothill) on both sides of the Rhône valley. Hourly records from 1993 to 2013 have been interpolated to a $0.1° \times 0.1°$ latitude–longitude regular grid and accumulated over 3-h periods in K-REF. The assessment of K-REF relatively to the SAFRAN daily rainfall reanalysis indicates consistent patterns and magnitudes between the two datasets even though K-REF fields are smoother. A multi-scale analysis of the occurrence and non-zero intensity of rainfall is performed and shows that the maps of the 50th and 95th percentiles of 3- and 24-h rain intensity highlight different patterns. The maxima of the 50th and 95th percentiles are located over plain and mountainous areas respectively. Moreover, the location of these maxima is not the same for the 3- and 24-h intensities. To understand these differences between median and intense rainfall on the one hand and between the 3- and 24-h rainfall on the other hand, we analyze the statistical distributions and the space-time structure of occurrence and intensity of the 3-h rainfall in two classes of days, defined as median and intense. This analysis illustrates the influence of two factors on the triggering and the intensity of rain in the region: the solar cycle and the orography. The orographic forcing appears to be quite different for the two ranges of the domain and is much more pronounced over the Cévennes.

Keywords Precipitation · Multi-scale climatology · Spatial analysis · Mountainous mediterranean region · MED-CORDEX · HyMeX

1 Introduction

This paper provides a climatology of the rainfall in Southeast France which should serve to assess rainfall output from Regional Climate Models (RCM).

The southeastern part of France, as most of the Mediterranean region, has a climate characterized by hot and dry summers and mild winters. In addition, several intense rain events have been documented in the region [Sénési et al. (1996), Delrieu et al. (2005), Ducrocq et al. (2008), Nuissier et al. (2008) for instance]. They can cause high impact floods with damages and casualties (Delrieu et al. 2005; Ruin et al. 2008). Moreover, the Mediterranean region is identified as one of the two main *"climate change Hot Spots"*, meaning it has one of the most sensitive climate response to global change (Giorgi 2006). In particular, summers are expected to be hotter and drier but with a higher variability, which leads to a rising likelihood of intense precipitation or drought (Giorgi and Lionello (2008), Giorgi et al. (2011), from data of the Coupled Model Intercomparison Project phase 3, CMIP3). Mariotti et al. (2015)

This paper is a contribution to the special issue on Med-CORDEX, an international coordinated initiative dedicated to the multi-component regional climate modelling (atmosphere, ocean, land surface, river) of the Mediterranean under the umbrella of HyMeX, CORDEX, and Med-CLIVAR and coordinated by Samuel Somot, Paolo Ruti, Erika Coppola, Gianmaria Sannino, Bodo Ahrens, and Gabriel Jordà.

✉ Stéphanie Froidurot
stephanie.froidurot@univ-grenoble-alpes.fr

[1] Laboratoire d'études des Transferts en Hydrologie et Environnement (LTHE), Université Grenoble Alpes/IRD/CNRS, 38000 Grenoble, France

Published online: 16 April 2016

confirm these conclusions thanks to an analysis of the CMIP5 run outputs. These climate projections result from the extensive use of Global Climate Models (GCM). Yet, the current spatial resolution of most GCM is of the order of few hundreds kilometers (Flato et al. 2013), which is usually too low to depict the impacts of climate variability at regional-to-local scales and develop adaptation strategies to deal with them (Giorgi et al. 2009). Therefore, downscaling methods are developed to provide finer-scale projections with greater details and more accurate description of localized processes (Hewitson and Crane 1996; Mearns et al. 1999; Maraun et al. 2010). Among the latter, RCM are able to simulate the long term climate evolution at resolutions as high as few tens of kilometers (Flato et al. 2013; Ruti et al. 2015).

Regarding the need of adaptation policies, it is important to know the confidence to give to climate projections and thus to evaluate the underlying models. In general, this evaluation is done comparing climate simulation results with observations over the far or recent past. For a proper assessment of simulated rain fields, simulated variables should be compared to observed ones at the same resolution. Skelly and Henderson-Sellers (1996) and Chen and Knutson (2008) showed that the characteristics of simulated rainfall can be very different depending on whether they are considered as point or areal quantities. Thus, it is important to use observational data at the appropriate scales for the evaluation of quantities highly variable in space and time such as precipitation. Using a multi-scale comparison of simulated rainfall with gridded observation, Chen and Knutson (2008) showed that climate models produce area-average-like rainfall outputs.

Therefore a number of gridded products of precipitation intensity have been developed, with various spatial and temporal resolutions matching model ones. Global products such as the CRU (Mitchell and Jones 2005), the GPCP (Huffman et al. 2001) or the CMAP (Xie and Arkin 1997) cover almost all the globe and are derived from ground based measurements sometimes supplemented by satellite data. These products have low spatial and temporal resolutions, ranging from 1° to 5° in latitude and longitude and from daily to monthly data. Such products from observational data are frequently used to evaluate large scale features in GCM and RCM [*e.g.* Dai (2006), Reichler and Kim (2008), Nikulin et al. (2012), Flato et al. (2013)]. In some regions of the world, databases provide rainfall fields at higher resolutions. Haylock et al. (2008) designed the E-OBS gridded database over central Europe. It gives daily data with spatial resolutions of about 25 and 50 km. Over France, the SAFRAN near-surface reanalysis (Quintana-Seguí et al. 2008; Vidal et al. 2010) gives daily and hourly estimations of several variables, including precipitation on a 8 km × 8 km grid. Yet, its subdaily rainfall is not computed from subdaily rainfall measurements but downscaled from daily data and it fails to diagnose some subdaily statistics such as the diurnal cycle of the rainfall intensity (Quintana Seguí 2008; Quintana-Seguí et al. 2008).

Multi-scale assessment of rainfall in climate models are seldom explicitly claimed. However, rainfall is a complex process in the sense that its statistical parameters vary as a function of scales. Therefore statistics at a unique spatio-temporal scale (*i.e.* 1 km^2–1 day for example) draw a partial picture of the phenomenon. The sensitivity of rainfall statistics to the scales is obvious when examining the relationship between the topography and the rain amount. For example, the highest rain depths are located over the mountain ranges at the annual, seasonal (Frei and Schär 1998) or daily time scales (Alpert 1986; Michaud et al. 1995; Johnson and Hanson 1995; Molinié et al. 2012). It is not the case when rain is aggregated on shorter periods (*e.g.* Johnson and Hanson 1995; Alpert and Shafir 1989). Multi-scale analysis is a current practice in applied extreme-rainfall statistics. An example is the set of Intensity–Duration–Frequency curves (Koutsoyiannis 1997) or Intensity–Duration–Area–Frequency curves (De Michele et al. 2001). These curves quantify the increase of the rainfall return level as the temporal and spatial scales of aggregation decrease. In the study region, Ceresetti et al. (2010) showed how the extreme rainfall pattern evolves with the temporal aggregation. A multi-scale analysis of rainfall in the study region may reveal the imprint of some atmospheric processes at the origin of different rainfall patterns. Flow-relief interactions play a major role in the organization of the banded orographic convection (Yates 2006; Godart et al. 2009). The associated rainfall is quasi-steady over the relief during several hours. Such rainfall events impact daily rainfall records while they are not significant on hourly ones (Molinié et al. 2012). The rainfall patterns due to deep convective systems often result from complex interactions between the relief and air flow dynamics and thermodynamics (Ricard 2002; Ducrocq et al. 2008; Nuissier et al. 2008; Fresnay et al. 2012). These systems can produce renewed rain cells for several hours either blocked over the foothill or advected in the Rhône valley or over the mountains. The associated rainfall captured by raingauges can be important both on hourly and daily time scales in the steady situation, or only high on hourly records when rain cells are advected. Molinié et al. (2012) showed that combining rainfall statistics at many durations permits to retrieve the signature of some underlying rain systems. Thus, if a multi-scale analysis of rainfall is needed to capture its complexity, it can also be used for a model evaluation in relation with the physical processes (Zepeda-Arce et al. 2000) or with the associated hydrological impacts (Yates et al. 2006; Ceresetti et al. 2012; Vié et al. 2012).

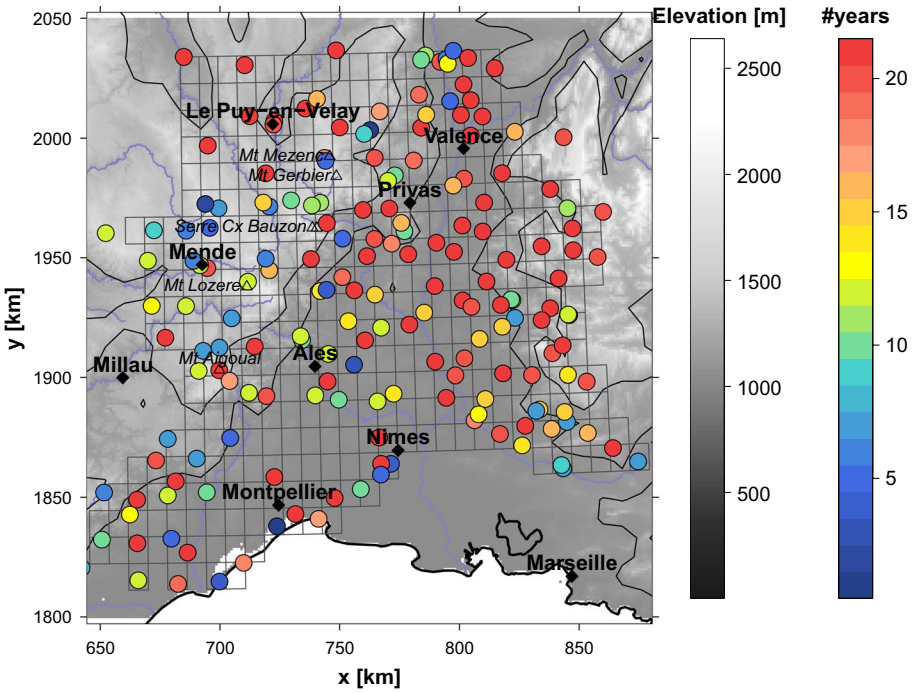

Fig. 1 Study region. The elevation is displayed in *shadings of gray*. The *black solid lines* correspond to the coastlines (*thick*) and to the 400 and 800-m elevation isolines (*thin*). Main cities and mountain tops are indicated by *diamonds* and *triangles* respectively, while *blue lines* stand for the main rivers. The *color-filled circle* specify the location of the hourly raingauges used in the study and the *grid boxes* show the grid on which data were interpolated. The *color of the circles* indicate the number of years of available data for each station

In summary, to perform a rainfall assessment of RCM, one needs a gridded database of rainfall at resolutions of about 10 km and 3 h which is nearly the highest resolutions of RCM in MED-CORDEX up to now. None of the datasets cited above supplies reliable subdaily rainfall. However due to its vulnerability to heavy rainfall, the survey of rainfall in the study region has been relatively sustained for several decades. We use these data to create a gridded rainfall database at the 10 km–3 h resolutions over Southeast France. The data and design of the database are described in Sect. 2 of this paper. A climatological study is then performed. The framework for rainfall characterization is detailed in Sect. 3. Rainfall is characterized by its occurrence and its intensity during rainy periods. We provide some statistics of the distribution of the rain occurrence for the 3-h accumulation period and proxies of its temporal structure in Sect. 4. Similarly the statistical distribution and temporal structure of rain intensity are showed in Sect. 5. Section 6 is dedicated to the spatial structure of both rain occurrence and intensity.

2 Data

2.1 Study area: Southeast France

The study region is located in the Southeast of France and covers an area of about $200 \times 200\,\mathrm{km}^2$ (Fig. 1). It is surrounded by the Mediterranean Sea to the south, the Massif Central to the northwest and the Alps to the east. The Rhône River flows across the domain, between the two mountain ranges. The southeastern border of the Massif Central is known as the Cévennes-Vivarais ridge delineated by several peaks, like Mont Aigoual (1565 m above mean sea level –MSL–), Mont Lozère (1699 m MSL), Mont Gerbier de Jonc (1551 m MSL) and Mont Mezenc (1753 m MSL) from south to north. The eastern side of the study domain consists of the Southern Alps foothills (including Vercors and Baronnies) and reaches about the same altitudes as the Massif Central Ridge.

The Cévennes-Vivarais area is subject to intense precipitation and flash floods (*e.g.* Delrieu et al. 2005; Nuissier et al. 2008; Ducrocq et al. 2008), mainly in autumn. Moreover, the whole region presents a very strong spatial precipitation gradient, with nearly 1000 mm of annual precipitation difference for example between Alès and Mont Aigoual that are only distant of about 40 km, but with 1400 m of height difference.

2.2 Hourly raingauges data

This study relies on hourly raingauges measurements from Météo France, the French meteorological service. Data are available from 1993 to 2013. Figure 1 shows the location of the raingauges over the studied area. The distance between neighboring raingauges ranges from 500 to 25 km, with a mean distance of about 8 km. The raingauges are rather well spread over the study region. The number of available measurements varies with time. Since 1993, it has increased from about several tens in 1993 to almost 150 in

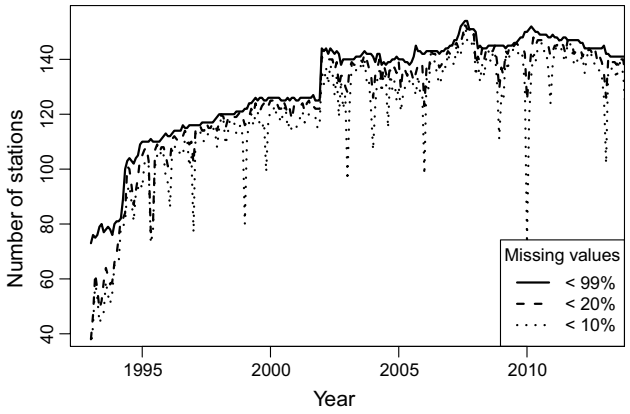

Fig. 2 Number of available stations with less than 99, 20 and 10 % missing observations per month

the 2010s as shown in Fig. 2. As for the location and the spatial spread of the stations, it stayed homogeneous along the study period. The number of years of available data for each station is presented on Fig. 1.

2.3 A spatial rainfall database

2.3.1 Design of the database

Rainfall outputs from climate models should be interpreted as areal averages (Chen and Knutson 2008). They cover periods as long as several tens of years. The only rainfall datasets recorded continuously during such long periods are the raingauge data. However, with sampling surface area of the order of 0.1 m^2, raingauge records are closer to point measurements when compared to RCM grid areas (of the order of 10^8 m^2). Due to the spatial variability of point rainfall inside each rain field, especially in the study region (non-stationnarity of the mean in Creutin and Obled (1982) for example), the statistical moments of the rain intensity evolve with the spatial integration. Therefore, the rain intensity recorded by a raingauge cannot be a similar random variable to the rain intensity in a surrounding grid box with a surface area that is a billion times greater. In the following, we describe a way of building a set of rainfall fields at the RCM spatial and temporal scales from point rainfall measurements, called K-REF hereafter (standing for *kriged reference*). In this manner, the rain depth in K-REF is a random variable comparable to the RCM rain depth. The raingauge data were interpolated (block kriging, see Chilès and Delfiner 1999, for example) to a $0.1° \times 0.1°$ latitude–longitude regular grid, in the range of the highest resolutions of the MED-CORDEX framework. We do not consider grid boxes outside the area delineated by the stations to avoid extrapolation from the data.

Kriging is a linear interpolation method. Thus, the rain depth estimated at some location x_0 (or on a grid box) $\hat{R}(x_0)$ is expressed as a linear combination of the observed rain depths $R(x_i)$ at the n locations of coordinates x_i (Eq. 1):

$$\hat{R}(x_0) = \sum_{i=1}^{n} \lambda_i R(x_i) \tag{1}$$

The linear coefficients of interpolation λ_i depend on the covariance of the interpolated random variable as a function of the distance. In this study, we used a climatological variogram as covariance function (Bastin et al. 1984; Lebel et al. 1987). This climatological kriging takes advantage of the large number of rainfall fields to infer the covariance function from the set of variograms of each individual field. Prior to computing the variogram, each rainfall field is normalized by its variance to account for the scale effect due to the variation in time of the mean rainfall intensity. However, a unique covariance function cannot characterize rainfall events that are too different. Thus, we split the rain events into eight groups based on the season and the spatial extent of rainfall. For each of the four seasons (DJF, MAM, JJA, SON), days with rain (called rainy days hereafter) are divided into two groups depending on the rain spatial extent, defined by the number of raingauges recording a precipitation amount (*i.e.* more than 0.1 mm). A rainy day lies from 06:00 UTC to 06:00 UTC the next day. In this study, rainy days with large spatial extent are those with more than 20 % of the raingauges wet. The kriging procedure is applied on the 3h-rain intensities, the shortest time step at our disposal in MED-CORDEX data. K-REF is then a set of rain depth fields from 1993 to 2014 kriged from hourly raingauges to $0.1° \times 0.1°$ grid boxes with a temporal integration of 3 h.

2.3.2 Evaluation of the database

We have chosen to assess the K-REF database in regard to its ability to describe not only the water resources but also the usual and intense rain intensities on short time steps. The rain generated water resource can be represented by the average annual rain depth. We use the 50th and 95th percentiles of daily rain intensity as proxies for usual and intense rain. These characteristics of K-REF are compared to those of the SAFRAN near-surface reanalysis (Quintana-Seguí et al. 2008; Vidal et al. 2010). SAFRAN is a reanalysis dataset commonly used for regional climate studies over France (for example in Boé et al. 2007; Quintana-Seguí et al. 2010; Chardon et al. 2014). The covered period ranges from 1958 to 2014. It has spatial resolution of 8×8 km^2 and we interpolated it to the same $0.1° \times 0.1°$ latitude-longitude regular grid as the kriged data using bilinear interpolation.

Figure 3 shows that the mean annual rainfall accumulation in SAFRAN and K-REF displays the same spatial structure. It is also consistent with previous studies performed on observations (Molinié et al. 2012, for example). The highest annual accumulations are located over the Cévennes-Vivarais mountain ridge. Despite some discrepancies, the average annual rain amount reaches about the same values in both datasets, around 1600 mm. This amount is much lower than the 2157 mm at Mont Aigoual reported in Molinié et al. (2012) from daily raingauges and than the 1988 mm at the same spot computed from the hourly intensities we use in this study. Such differences, between an areal average and point values on the one hand and between point values not covering the same time period and not located exactly at the same place on the other hand, suggest a relatively high variability of the rain in the surrounding of the mountain ridge. The average annual rainfall at the three closest stations to Mont Aigoual in the hourly dataset corroborate this variability. All are located within 10 km of Mont Aigoual and they feature average annual depths of 1296, 1275 and 818 mm. The spatial variability of rain events is smoother in SAFRAN and K-REF than in the raingauge records because of the spatial aggregation, and even smoother in K-REF as showed in Fig. 3. The differences in the interpolation methods and the network density used to produce SAFRAN and K-REF might be the main reasons for the K-REF fields to be smoother than the SAFRAN ones. Indeed, the optimal interpolation method used in SAFRAN is different from that of K-REF (Quintana-Seguí et al. 2008) and the decorrelation distance in K-REF (several tens of kilometers guessed from 3-hourly data) may be longer than in SAFRAN. Moreover, SAFRAN relies on daily rain gauges, more numerous than the hourly ones used in K-REF and thus more prone to catch the rainfall heterogeneity.

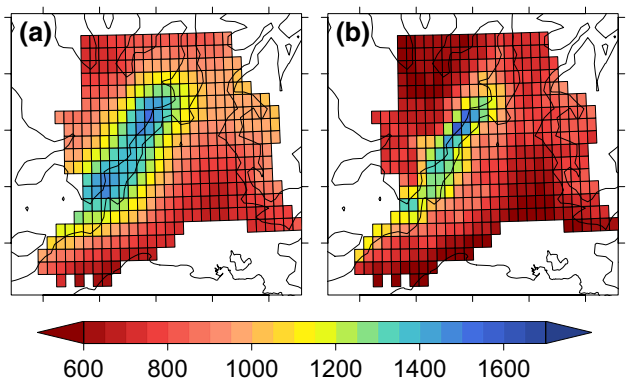

Fig. 3 Mean annual rainfall accumulation in mm for the 1993–2013 period (**a**) from the 3-hourly kriged rainfall and (b) from the SAFRAN data. The *black solid lines* corresponding to the coastlines (*thick*) and to the 400 and 800-m elevation isolines (*thin*) are the same as in Fig. 1

In both databases, the rain accumulation decreases with the terrain elevation either from the Cévennes or the Alps to the Rhône river valley. In the valley, the mean annual rain amounts are around 700 mm in both databases. This value is comparable to the 760 mm of rain recorded, in average, each year at the raingauge of the city of Nîmes (about 30 km from the Mediterranean sea).

According to Molinié et al. (2012), the distributions of daily intensities are different from one raingauge to another in the region. In the following, we compare two percentiles of the distributions of the daily rain accumulations in both databases. The comparison of the 50th and 95th percentiles of non-zero daily rain depth between the two datasets is shown in the first two rows of Figs. 4 and 5 for each of the four seasons. Non-zero rain depth are defined as precipitation above 0.1 mm during the considered accumulation period, which is also the detection threshold of the raingauges. The 50th percentiles of the K-REF daily precipitation are consistent with that of SAFRAN. The locations of the highest median values are quite the same: over the Alps foothills for all seasons except summer. For both datasets, autumn (SON) features the highest median depths and summer (JJA) the lowest. The smoothing due to the kriging already discussed also appears on these maps. The values are lower in the kriged data than in SAFRAN and the patterns are smoother. For example, the maximum median depths, encountered in the Alps foothills, reach 3.5 mm in K-REF and more than 4 mm in SAFRAN.

The patterns of the K-REF daily precipitation 95th percentiles are similar to that of SAFRAN. In spring (MAM), autumn (SON) and winter (DJF), the highest values are located over the Cévennes relief while in summer (JJA), they are over the Rhône Valley. Among the four seasons, autumn is the one with the highest values of 95th percentile both in K-REF and SAFRAN data. In autumn, over the Cévennes mountain ridge, the 95th percentile of daily precipitation amounts to about 60 mm in K-REF and more than 80 mm in SAFRAN. In summer, the maximum values of the whole region are about 30 and 35 mm in K-REF and SAFRAN respectively. The smoothing in the kriged data appears again, with lower values and a smoother pattern in K-REF than in SAFRAN. It can also be noted that the location of the highest 95th percentiles of daily precipitation over the Rhône Valley in summer appears less clearly in SAFRAN.

3 Framework for rainfall characterization

In the following, we characterize rain in each grid box of K-REF by the occurrence and the non-zero intensity,

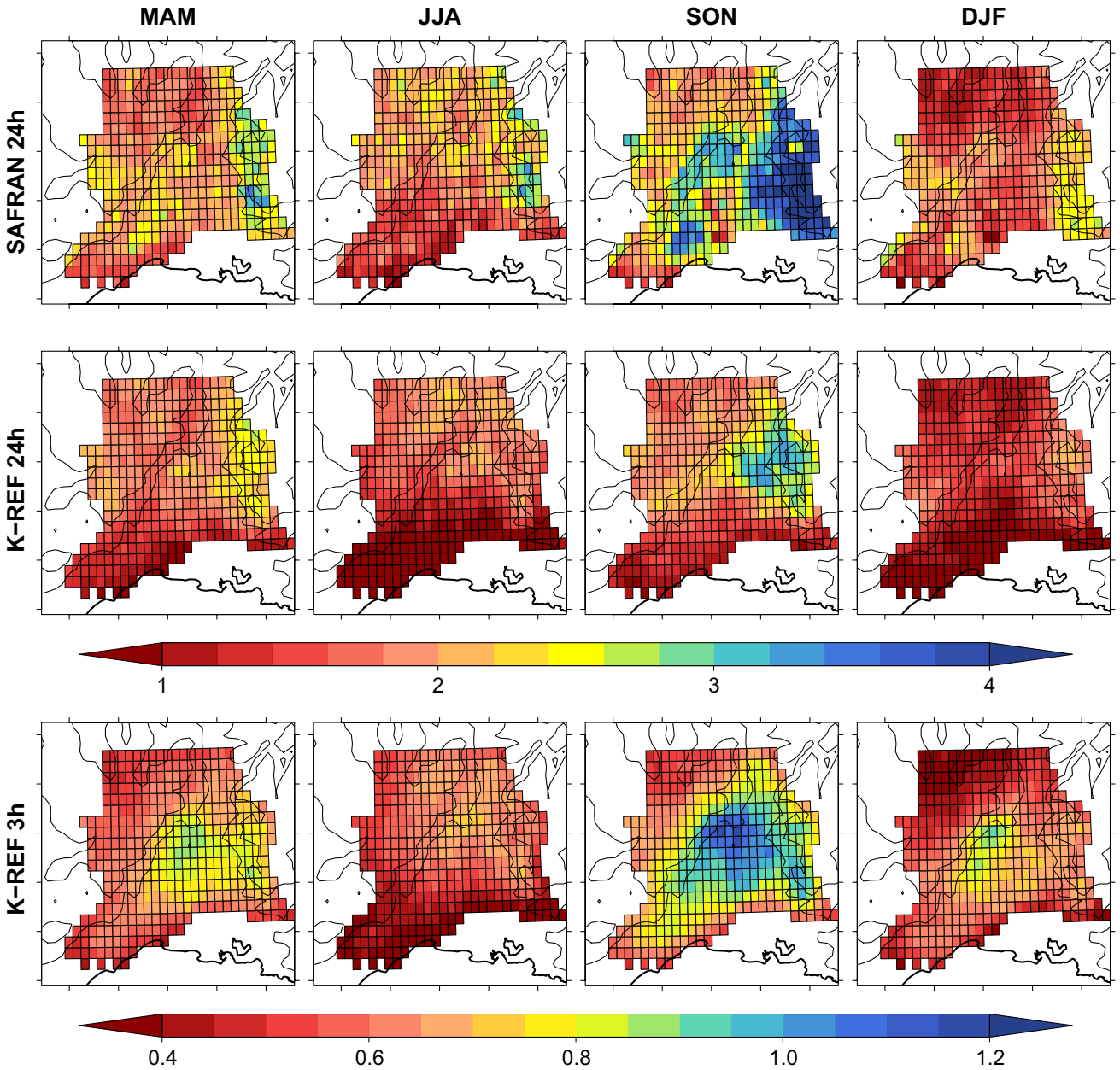

Fig. 4 50th percentile of non-zero daily rain depth for each *grid box*, for the four seasons in SAFRAN (*top*) and K-REF (*middle*). 50th percentile of non-zero 3-h rain depth in K-REF (*bottom*). Non-zero rain depths are defined as rain depths above 0.1 mm. See Fig. 3 for more caption details. Units are mm

hereafter referred to as the rain intensity for simplicity. For a given accumulation period, occurrence is the fraction of rainy periods among all the periods.

The non-zero intensity is the rain intensity during rainy periods. A random variable (occurrence or intensity, here) is fully characterized by its statistical distribution. As there are hundreds of grid boxes in K-REF, it is impossible to study all quantiles in all the distributions. We will focus on the usual (median, 50th percentile) and heavy (95th percentile) intensities. To depict a comprehensive picture of rainfall and take its scale dependency into account, the analysis of the spatial and temporal structure of the occurrence and intensity fields complement their statistical distributions.

An illustration of the scale dependency of the occurrence and intensity is given by the comparison of the 50th and 95th percentiles of non-zero rain depth for accumulation periods of 3 and 24 h (Figs. 4 and 5). Figure 4 shows how the highest median intensities switch from the west of the Rhône valley to the Alps foothills (east of the valley) when the accumulation period increases from 3 to 24 h, during

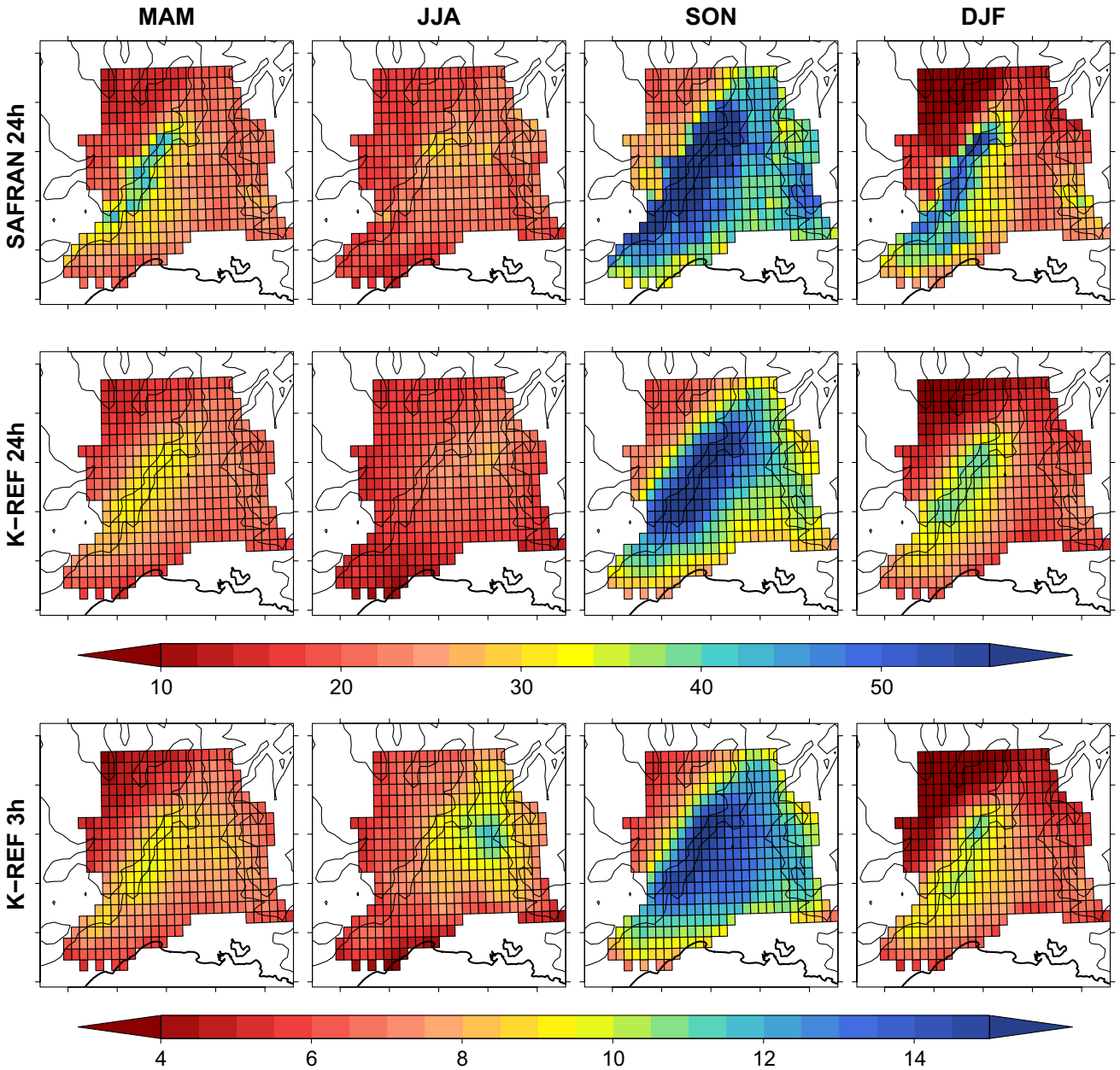

Fig. 5 95th percentile of non-zero daily rain depth for each *grid box*, for the four seasons in SAFRAN (*top*) and K-REF (*middle*). 95th percentile of non-zero 3-h rain depth in K-REF (*bottom*). Non-zero rain depths are defined as rain depths above 0.1 mm. See Fig. 3 for more caption details. Units are mm

all seasons except summer. In summer, the highest values remain in the valley both for the 3- and 24-h accumulation period. Concerning the 95th percentiles (Fig. 5), the maximum depths are, on the whole, at the same location at 3 and 24 h. However, in autumn, the highest values extend to the Rhône valley for the 3-h accumulation period, which is not the case for daily precipitations. Moreover, if summer is the season with the lowest 95th percentiles of daily rain depths, it is not the case for the 3-h ones and quite large values are observed in the north of the Rhône valley.

Comparing rain depths between two accumulation periods (3 and 24 h) provides similar information than assessing the temporal structure of the rain depth between these two periods. However, structure functions such as correlograms or variograms can be computed for a continued range of accumulation periods and thus have a generic meaning. In the following, rather than systematically comparing rain parameters at two accumulation periods, we characterize the elementary parameters of rainfall available in this study, *i.e.* occurrence and intensity at the 3-h accumulation

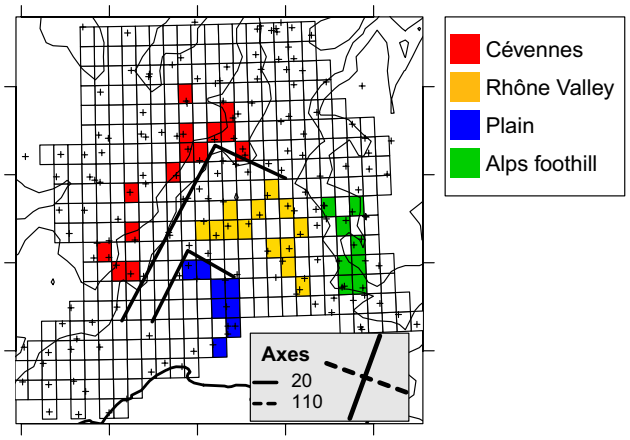

Fig. 6 Localisation of the *grid boxes* of each of the four subregions: Cévennes in *red*, Rhône Valley in *yellow*, plain in *blue* and Alps foothills in *green*. The limits utilized in Miniscloux et al. (2001) are drawn over the map. The main directions (20° and 110° to the north) used to study the spatial structure of rainfall in Sect. 6 are indicated in the box in the *bottom right corner*. See Fig. 3 for more caption details

period and their temporal structure. We conduct this analysis in order to depict how the rainfall basic elements (3-h rain depths in this study) combine to produce the daily rain depths. To do so, we focus on the organization of 3-h rain occurrence and intensity during median and intense days. For each grid box, *Median days* are defined as days with a rain depth recorded during a 24-h period from 6:00 UTC lying between the 40th and the 60th percentiles of its non-zero daily rainfall. *Intense days* are taken between the 85th and 98th percentiles. These percentile ranges are chosen to include the percentiles studied previously (50th and 95th) and are trade-offs between robustness and distinctiveness: they have to be wide enough for the statistics to be robust and narrow enough not to mix events that would be too different.

The study region is divided into four subregions represented in Fig. 6: *Cévennes*, *Rhône valley*, *plain* and *Alps foothill*. In each subregion, the analysis is conducted on a number of selected grid boxes located in well-defined topographical features and containing at least one gauge. Among these subregions, *Cévennes* and *Alps foothill* are mountainous areas, their main slopes face respectively east-southeast and west. The two other subregions, *Rhône valley* and *plain* are predominantly flat sectors. They differ on their mean altitude. The *plain* extend from the Mediterranean shore to the city of Alès approximately and is mainly below 200 m. The *Rhône valley* subregion is principally between 200 and 500 m. The three subregions at the west of the Rhône river were already defined in Miniscloux et al. (2001) to study the structure of shallow clouds yileding rainfall. Ceresetti et al. (2012) only used the Cévennes mountain/foothill delineation to compute scaling parameter of extreme rainfall.

In Sects. 4 and 5, we examine the seasonal and regional variability of rainfall occurrence and intensity. The time structure is investigated by means of the diurnal cycles. The spatial structure of occurrence and intensity are studied in Sect. 6.

4 Subdaily rain occurrence

This section is devoted to the rain occurrence at the resolution of 3 h. Figure 7a shows the mean rain occurrence during rainy days depending on the season, the type of day (*i.e.* median or intense) and the subregion considered. The occurrence of rainfall unsurprisingly depends on the season and on the type of day but less of the subregion, except for the *Cévennes*. While between 25 and 45 % of the 3-h periods are rainy during median days, it rains more than 50 % of the time during intense days. Rain in summer is the most intermittent. The mean occurrence of rain is lower by about 15

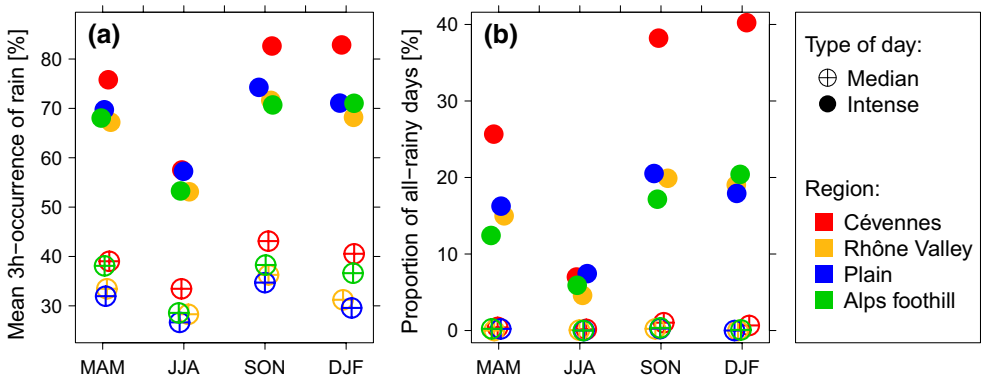

Fig. 7 **a** Fraction of rainy periods among all the 3-h accumulation periods and **b** fraction of days with 8 rainy time steps of 3-h during each of the four seasons, depending on the type of day (median or intense) and the subregion considered

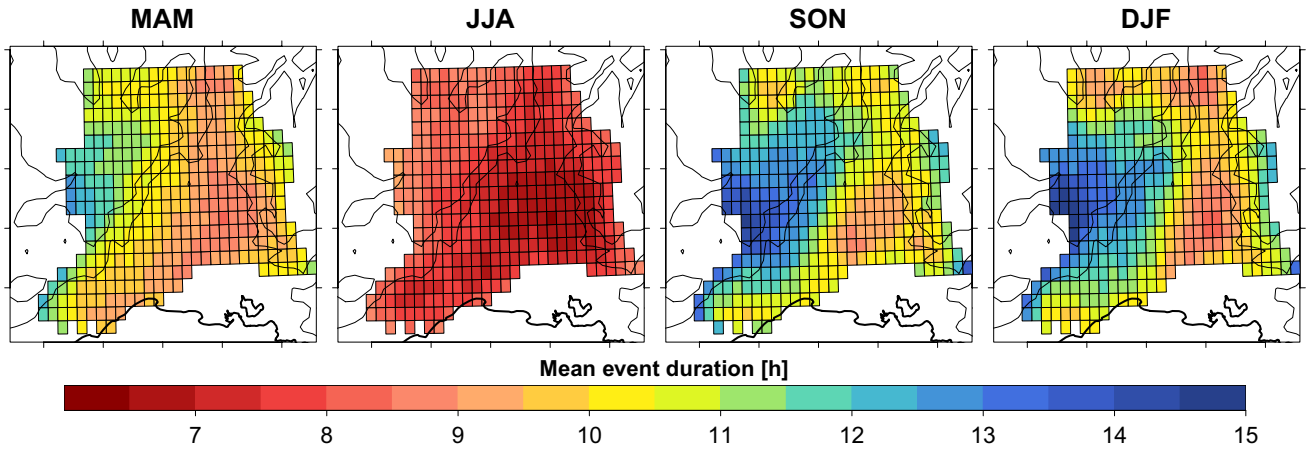

Fig. 8 Mean duration (in hours) of rainy events for each of the four seasons (MAM, JJA, SON, DJF). See Fig. 3 for more caption details

percentage points in comparison with the other seasons. The Cévennes subregion has a behavior distinguishable from the other subregions, principally during intense days, except in summer. In autumn for example, during intense days, it rains more than 80 % of the 3-h periods in the Cévennes when it is only about 70 % of the time elsewhere. It is worth noting that this difference between the Cévennes subregion and the other ones is enhanced when considering the fraction of all-rainy days, which we define as days with continuous rain at the 3-h resolution, in other words days with 8 rainy 3 h-periods out of 8 (Fig. 7b). In autumn and winter, almost 40 % of the intense days are all-rainy days in the Cévennes when they are only about 20 % in the other subregions. In summer, there are fewer all-rainy days, even among intense days (less than 10 %) whatever the subregion considered.

The mean duration of the rainy events provides a first assessment of the temporal structure of the rain occurrence. Rainy events are defined as a series of successive 3-h rainy periods, *i.e.* 3-h periods with more than 0.1 mm of rain depth. Figure 8 shows event duration for four seasons. The shared character between the seasons is the gradual increase of event duration over the mountain slopes both on the Cévennes and the Alps sides (even if our description is limited to the Alps foothill). The difference between the Rhône valley and the Cévennes ridge is noticeable. In autumn for instance, there is 9 h of consecutive rain in average in the plain (*i.e.* 3 consecutive periods of 3 h with at least 0.1 mm of rain) while it reaches 15 h over the Cévennes ridge, especially near Mont Aigoual. As expected, rainy events are shorter in summer, lasting 6 to 9 h on average, than during the other seasons. Moreover, the pattern of the event lengths in summer shows a delineation by the Cévennes ridge while it is centered on that ridge during the other seasons.

Then, the temporal structure of rain occurrence is examined through its diurnal cycle to describe how the rainy periods are organized along rainy day. Depending on the season and the type of day, the cycles are more or less marked. Figure 9 shows the diurnal cycle of the normalized rain occurrence in each subregion, during the median and intense days of the four seasons. For normalization purpose, the rain occurrence of each time slot is divided by the daily average occurrence. The standard deviation of the normalized occurrence in each subregion is represented on both sides of the average in order to assess the occurrence variability. Whatever the season, intense days are characterized by a clear diurnal cycle with low variance within the subregions and between the subregions. On the other hand, during median days, cycles are only marked in spring and summer. In autumn and winter, the diurnal cycles are less obvious and with a high variability within the subregions. In all the cases, when rain occurrence shows a clear diurnal cycle, the associated peak is observed during the afternoon, at 18H UTC (seldom at 21H UTC).

This analysis of the rain occurrence shows the importance of two processes to trigger rainfall. On the one hand, the mean occurrence of rainfall being higher in the *Cévennes* than elsewhere (Figs. 7 and 8) suggests the role of interaction between the air thermodynamics and the relief. This is particularly true during intense days (except in summer). On the other hand, the marked diurnal cycle of rain occurrence (Fig. 9) highlights a forcing associated with the hour of the day. Therefore, the solar energy should have a specific importance. It is noticeable that such a forcing affects the overall region. Various studies suggest that the rain occurrence peak in the afternoon is associated with boundary layer destabilization due to daytime insolation (*e.g.* Nesbitt and Zipser 2003; Dai et al. 2007; Mandapaka et al. 2013). Solar heating at the surface produces sensible and latent heat fluxes from the surface into the boundary layer, making the atmosphere conditionally unstable locally and convection can initiate more easily. However,

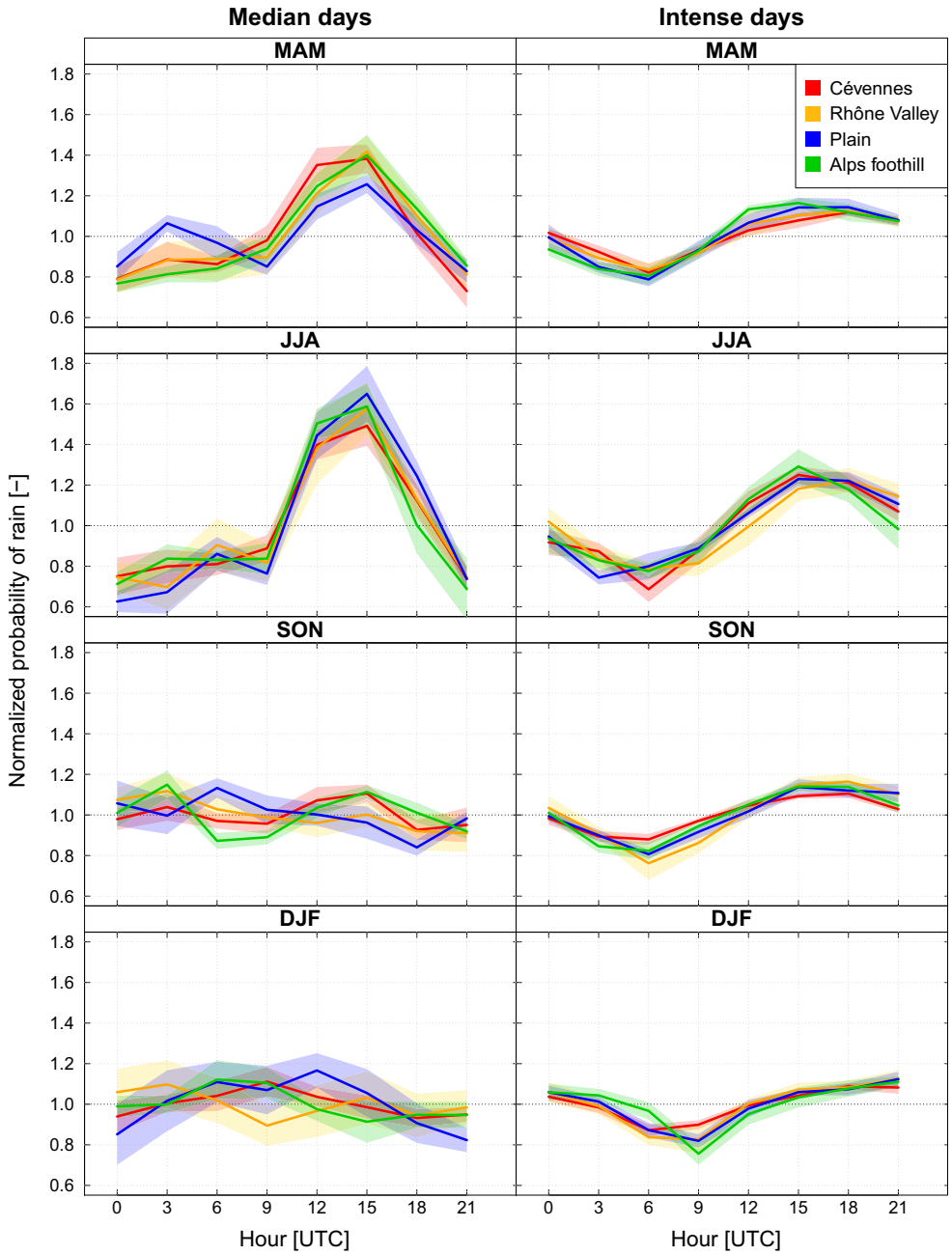

Fig. 9 Diurnal cycle of rain occurrence for the four seasons (MAM, JJA, SON, DJF) and for each subregion (*color*) during median (*left*) and intense days (*right*). *Solid lines* are the mean probabilities of rain for every time slot in each subregion, normalized by the daily mean. The standard deviation of the values in each subregion are represented on either side of the mean value

solar heating can also induce variations in the atmospheric circulations from the local to the large scales (Oki and Musiake 1994; Dai et al. 1999; Biasutti et al. 2012, among others). At the regional scale, sea breeze can influence the rain occurrence diurnal cycle. In the study region, under low synoptic forcing the sea breeze can penetrate inland (Bastin et al. 2005) and propagates along the Rhône river valley (Drobinski et al. 2006). The role of the sea breeze in favoring the initiation of rainy clouds has been demonstrated since several decades (in Florida, for instance in Pielke 1974) and can be associated with an afternoon peak in the statistics of the rain occurrence (Hill et al. 2010). However, questions remain on the timing. Drobinski et al. (2006) show that the location of the sea breeze front is not synchronous from one day to another. Given the spatial and temporal resolution and the spatial extent of the subregions used in the present study, a clear identification of the processes associated with the sea breeze seems

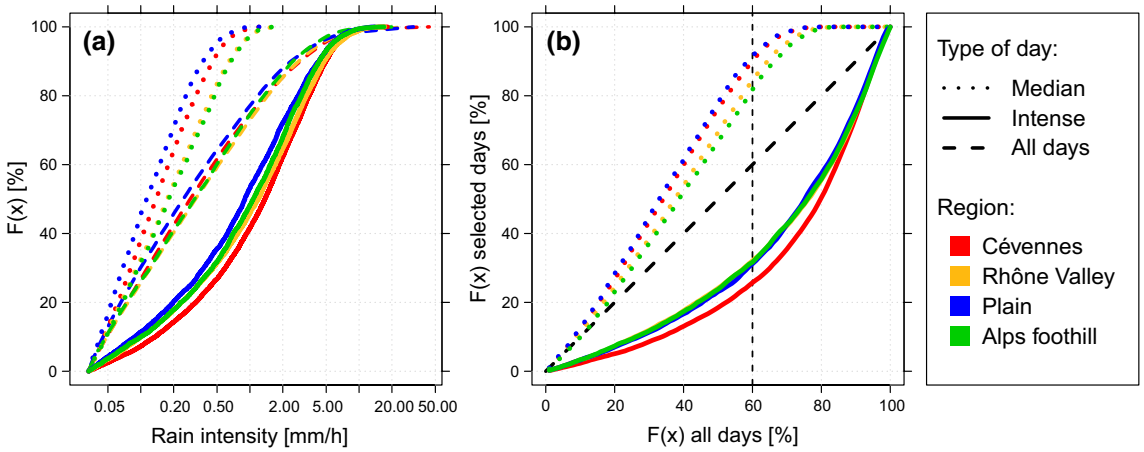

Fig. 10 **a** 3h-rainfall empirical cumulative distribution in autumn, for each subregion (*color*) if all the days are taken into consideration (*dashed line*), during median (*dotted line*) and intense (*solid line*) days. **b** Non-exceedance frequencies of the 3-h intensities in median and intense days (selected days) with respect to that in the whole of the days

hardly possible. Further investigations are then necessary to draw the whole picture of the processes involved in the rain occurrence diurnal cycle and of the importance of the sea breeze front specifically.

5 Subdaily rainfall intensity

In the previous section, we showed the organization of 3-h rainy periods during median and intense days. In this section, we characterize the intensities of these rainy periods. Figure 10a shows the cumulative frequency distributions of the 3-h intensity during median and intense and the whole set of days for the four subregions, in autumn (the other seasons have a similar behavior). Because of the wide range of intensities, a log-scale is used for the x-axis.

As expected, median days are prone to lower intensities than intense days. Moreover, regarding the whole set of 3-h intensities, those composing the intense days are among the largest. Combining this result with that of Fig. 7, intense rainy days are both less intermittent and made up of the heaviest 3-h intensities. Comparing the subregions, the plain is more likely to have the lowest 3-h intensities both in median and intense days. Combined to the highest intermittency during rainy days (Fig. 7a), the plain is the less watered of the subregions, whatever the time scale considered (3 h, day, year). However, it can seldom feature among the highest 3-h intensities, the tip of its distribution reaching 30 mm/h in 3 h, a rate only exceeded in the Cévennes subregion with about 40 mm/h recorded in 3 h. Deep convection generated because of a low-level cold pool, such as the one associated with the Gard flash flood event described in Ducrocq et al. (2008), may provide such extreme rainfall. Delrieu et al. (2005) report an average of 40 mm/h recorded during 6 h over the plain on September 9, 2002. For the other three subregions, the relative order of the cumulative distributions change between the median and the intense days. The Cévennes subregion seems to switch from the lowest to the highest value of the cumulative distribution between the median and intense days. For any given quantile, it has among the lowest 3-h intensities during median days and the highest during intense days.

Such a comparison of the 3-h intensities portraits only a partial picture of the subregion differences. Indeed, the distributions of 3-h intensities in the whole set of days are different from one subregion to another as illustrated by Figs. 4, 5 and 10a. Thus, the distribution of intensities during selected (median or intense) days are expected to be different. To filter out this effect, Fig. 10b is similar to Fig. 10a but the x-axis is replaced by the cumulative frequency in the whole set of 3-h intensities for each subregion. It emphasizes the features revealed in Fig. 10a. First, median days are made of the lowest 3-h intensities, specifically the highest 20 % of the 3-h intensities never occur during these days. Second, the Cévennes subregion is the most likely to have low 3-h intensities than the other subregions during median days. Around 90 % (compared to 81 and 84 % in the Alps foothill and the Rhône Valley) of the 3-h intensities of median days are drawn from the lowest 60 % of the whole set of 3-h intensities. On the contrary, the intense days are made of the highest 3-h intensities, more particularly in the Cévennes. For instance, 75 % of the 3-h intensities are drawn from the highest 40 % of the whole set of days while it is only about 68 % in the other subregions.

Since we have now characterized the values of the 3-h intensity, we study their temporal structure by the mean of the diurnal cycle of their median (Fig. 11). To facilitate the

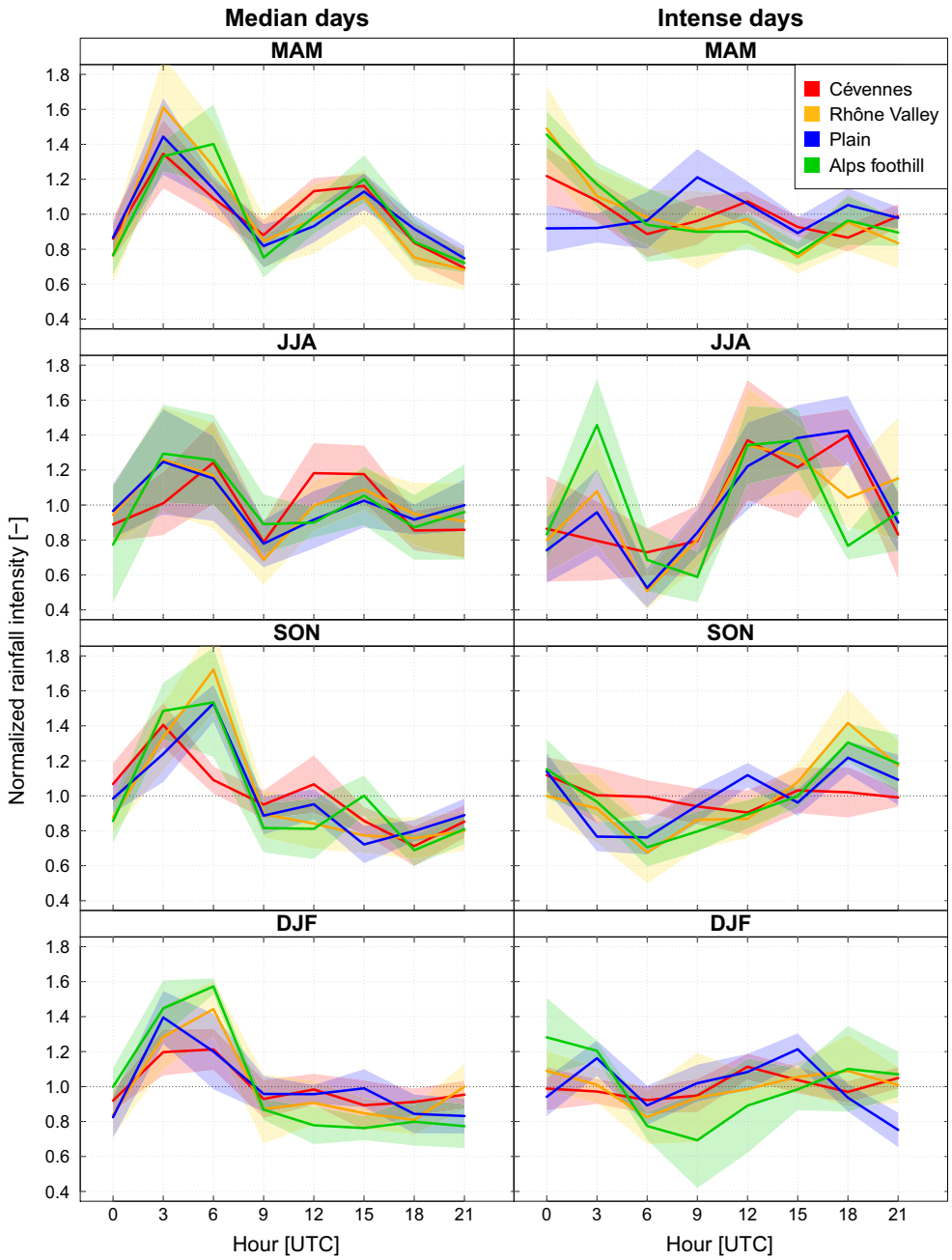

Fig. 11 Diurnal cycle of the 3-h rain intensity for the four seasons (MAM, JJA, SON, DJF) and for each subregion (*color*) during median (*left*) and intense days (*right*). *Solid lines* are the average of the median rain intensities for every time slot in each subregion, normalized by the daily mean of the cycle. The standard deviation of the values in each subregion are represented on either side of these *lines*

comparison between subregions and seasons, the median are normalized by their daily average. On the whole, the intensity cycles are less clear than those of occurrence. However, some general features emerge like a maximum of the intensities in the morning during median days. An additional intensity peak appears in the afternoon in MAM and JJA, correlated to an occurrence peak. These observations during median days question the existence of physical processes accentuating rain intensity in the morning, independently of the occurrence and in the afternoon in conjunction with the rain occurrence peak. Further investigation is needed to elucidate the processes behind this morning peak.

Most of the time, intense days are characterized by a diurnal cycle of intensity. Autumn intense days in the Cévennes subregion, where the most intense events may

occur, is a counter-example. The intensities do not depend on the hour of the day. In this case, the solar forcing does not seem to have a primary influence on these intensities.

6 Spatial structure of rainfall

The comparison of the distribution and temporal structure of the rain occurrence and intensity between the four subregions has highlighted some specific behaviors in relation to the relief and to the diurnal cycle. We analyze now the spatial structure of the 3-h rain occurrence and intensity. The correlogram and variogram are classical statistics of a random function structure. The latter offers the advantage of filtering the spatial trend of the analyzed statistics. Throughout this article we show that rainfall statistics vary gradually in space, like the average annual rainfall (Fig. 3), the 3- and 24-h 95th percentile of rainfall (Fig. 5) or the rain event duration (Fig. 8). Therefore, the variogram is worthwhile (Delhomme 1978; Chilès and Delfiner 1999, p. 115). When computed for the whole set of grid boxes, the variogram does not provide meaningful information, certainly because the rain features are very dependent on the subregions. Thus, in the following, the variogram is applied in the neighboring of a set of gridboxes, when they are wet, using Eq. 2. It provides an estimation $\hat{P}(h)$ of the no-rain probability at a distance h from a rainy gridbox.

$$\begin{aligned}\hat{P}(h) &= \frac{1}{n}\sum_{i,j\in\mathcal{E}}\left(Occ(x_j) - Occ(x_i)\right)^2 \\ \mathcal{E} &= \left\{i,j | dist(x_i,x_j) \in [h-\delta, h+\delta] \text{ and } Occ(x_j) = 1\right\} \\ &= \frac{1}{n}\sum_{i,j\in\mathcal{E}}(1 - Occ(x_i))^2 \end{aligned} \quad (2)$$

where $Occ(x_i)$ represents the occurrence of rainfall (1 if it rains, 0 if not) at any grid box of coordinates x_i, distant of h with a tolerance δ around h from a rainy gridbox of the considered subregion (x_j). In order to provide synthetic quantitative assessment of the behavior of the no-rain probability as a function of the distance, we fit spherical models on the $\hat{P}(h)$ values. In geostatistics, such spherical models are used to fit semi-variograms (Chilès and Delfiner 1999, p. 104). In particular, these models are commonly used in the literature to describe the spatial structure of rainfall statistics at ranges beyond the kilometer (*cf.* Creutin and Obled (1982); Lepioufle et al. (2012); Leblois and Creutin (2013) among others). Equation 3 is the spherical model of the no-rain probability P at distance h from the selected rainy grid box:

$$P(h) = \begin{cases} N + S\left(\frac{3}{2}\frac{h}{R}\right) - \frac{1}{2}\left(\frac{h}{R}\right)^3 & \text{if } 0 \le h \le R \\ N + S & \text{if } h \ge R \end{cases} \quad (3)$$

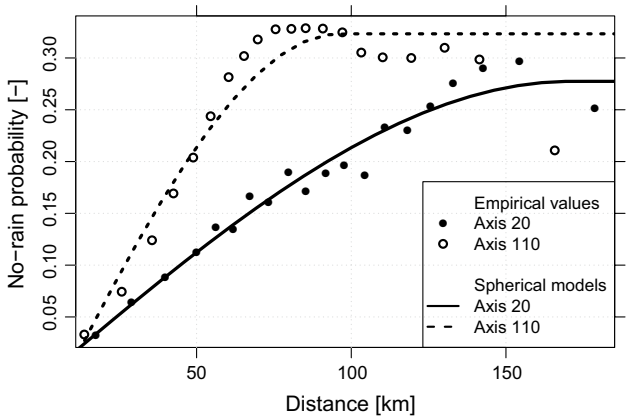

Fig. 12 No-rain probability in relation to the distance to a rainy *grid box* in the Cévennes subregion, during autumn intense days. *Filled* and *open circle* indicate the empirical values along the directions axis 20 and 110 respectively. The corresponding directions are shown in Fig. 6. Spherical models are calibrated on the empirical values and are shown in *solid* (axis 20) and *dashed* (axis 110) *lines*

This model states that the no-rain probability is about N, the nugget, close to the selected grid box. N accounts for the local variability which is often due to measurement uncertainties. The probability of no-rain increases continuously with the distance up to the range distance R. The so-called range R indicates the decorrelation distance of the no-rain probability and could be considered as a proxy for the size of the rainy zones. The sill $N + S$ relates to the no-rain probability beyond the range.

Figure 12 shows the evolution of the no-rain probability with the distance to a rainy gridbox of the Cévennes subregion along two main directions (see Fig. 6), in autumn. These two directions are chosen tangential and perpendicular to the Cévennes relief. They were also shown by Miniscloux et al. (2001) to be major axes for orographic banded convection events. Results are shown for intense days. The conclusion are similar for median days. Following the mountain ridge direction (axis 20), the range is about 170 km when it is only about 95 km in the perpendicular direction (axis 110). The no-rain probability beyond the range is 28 % in the direction parallel to the mountain ridge when it is of 32 % in the perpendicular direction.

Figure 13 displays the parameters of the spherical models of all the seasons and subregions along these two main directions (axes 20 and 110) in order to specify the possible influence of the Cévennes relief on rainfall patterns. Sills and ranges are larger in the Cévennes subregion than in the other ones. The rainy zones are more extended but the probability of rain outside of these zones is lower. This is again in agreement with the triggering role of the mountain. Moreover, it can be noted in Fig. 13b that all the points are over the bisector. It means that the ranges are larger in the direction of the mountain ridge than in the perpendicular

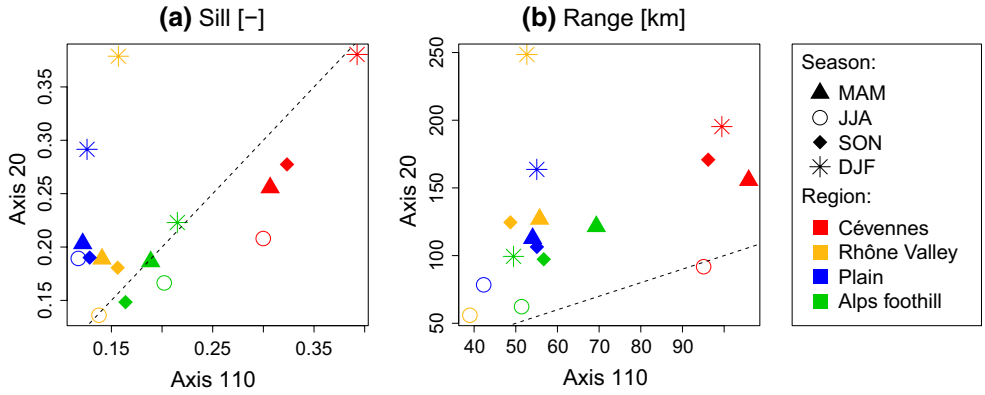

Fig. 13 Sill (**a**) and range (**b**) of the spherical models calibrated on the variation of the no-rain probability with the distance to a rainy *grid box* during intense days. The structure is studied around the *grid boxes* of the four subregions, indicated by the *colors* of the points. Each of the four seasons is represented by a *different symbol*. The *dashed line* is the bisector line, in other words, where the values are the same for the two axes

one. In summer, in all the subregions, the ranges are shorter than during the other seasons and with closer values in the two directions, indicating smaller and rounder rain cells. The relief seems to be of high importance in the spatial structure of intermittency but this effect is lower during summer.

Figure 14 allows to visualize the likely rain patterns but focuses on three specific grid boxes (red crosses). The color scale indicates the no-rain likelihood whithin a 3-h period when the red cross location features either a median or an intense day. The three reference grid boxes are located in the Cévennes subregion, the Alps foothill and the south of the Rhône Valley (representative of the Rhône Valley and the plain subregions). These patterns of the rain area boundaries are shown for autumn and summer. Winter and spring features rainfall occurrence structures close to that of autumn. In summer, the occurrence structure is almost the same during intense and median days, except with less occurrence during median days. The same patterns of the no-rain probability can be found during median autumn days. They are fairly anisotropic in the neighborhood of the studied grid boxes. Conversely, during intense days of autumn, the occurrence patterns are more extended and anisotropic than during autumn median days or summer days. The studied grid box in the Cévennes (left column of Fig. 14) is located close to Mont Aigoual (1565 m). Like Mont Lozère, Mont Gerbier de Jonc and Mont Mezenc, all of them situated along the Cévennes ridge, Mont Aigoual is the major obstacle of the low-level flow in two sectors: south to east and southwest to northwest. It is interesting to notice in Fig. 14j the particularly high rainfall likelihood in these sectors, specifically in the south to east one where the rain likelihood is of more than 80 % several kilometers away from Mont Aigoual. Another interesting feature is the high level of rain likelihood along the Cévennes ridge. When it rains at Mont Aigoual, the concomitance of rain both over the southern to eastern slopes of the Cévennes and over the ridge is typical of some heavy rain events of the region. There are in the literature review two types of rain systems that may provide such features of the rain occurrence. Meso-scale convective systems (MCS), initiated over the southeastern slope of the Cévennes by low-level jets of instable air, water both the Cévennes foothill, the slopes and the ridge where deep convective cell may occur (Ricard 2002; Fresnay et al. 2012). Stationary orographic rain-bands initiated under a weaker southern flux with respect to MCS (Godart et al. 2010) is the other type of system. This type of system yields daily rain amounts in the range of those of intense days as they are defined in the present study (Miniscloux et al. 2001; Godart et al. 2011). Shallow convective cells are stationary over the ridge and also produce rain over the slope (Yates 2006).

Around the plain grid box (central column in Fig. 14), the structure is oriented toward the northwest. It can be due to specific atmospheric circulations that would deserve further investigations. Berne et al. (2009) show that MCS traveling northward over the Rhône valley yield such an occurrence pattern. Beyond the range of the rain probability, 110 km in the 20° North direction and 55 km in the 110° North one (Fig. 13), the likelihood of rain concomitant everywhere in the region is higher than when it rains over the Alps foothill and significantly higher than when it rains in the Cévennes.

To supplement the study of the structure of rain occurrence, the organization of rainfall intensity is discussed in the following. Figure 15 shows the same kind of analysis as in Fig. 14 but for rain intensity. The intensity differences are computed between each grid box and the reference one when both are rainy. The median of these differences is shown for each grid box in Fig. 15 for summer

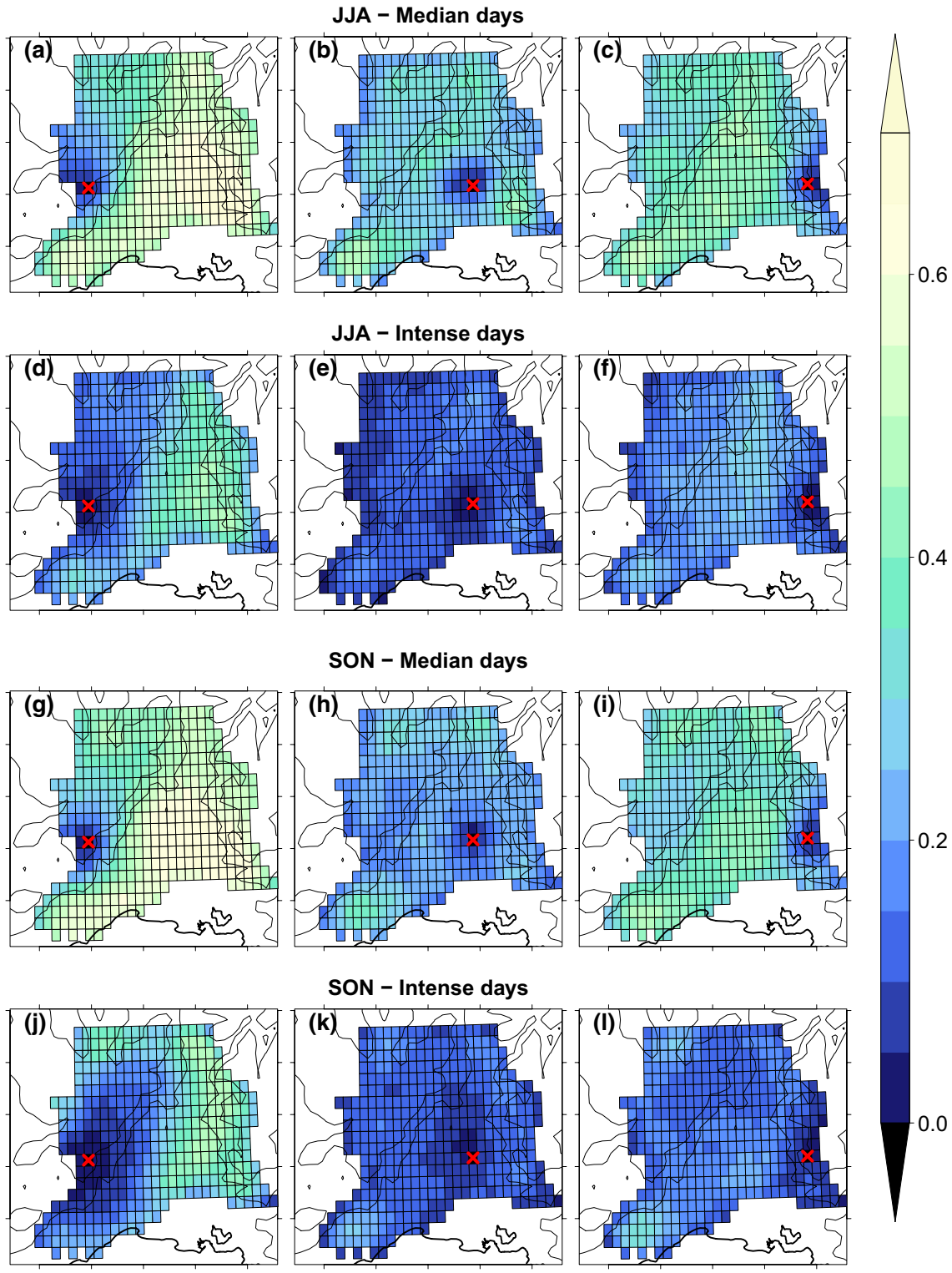

Fig. 14 Spatial repartition of the no-rain probability, knowing that a certain *grid box* (*cross*) is rainy during summer median (**a**–**c**) and intense (**d**–**f**) days and autumn median (**g**–**i**) and intense (**j**–**l**) days). The reference *grid boxes* (*red crosses*) are located in the Cévennes subregion (*panels* **a**, **d**, **g** and **j**), the Rhône Valley area (**b**, **e**, **h**, **k**) and the Alps foothill (**c**, **f**, **i**, **l**). See Fig. 3 for more caption details

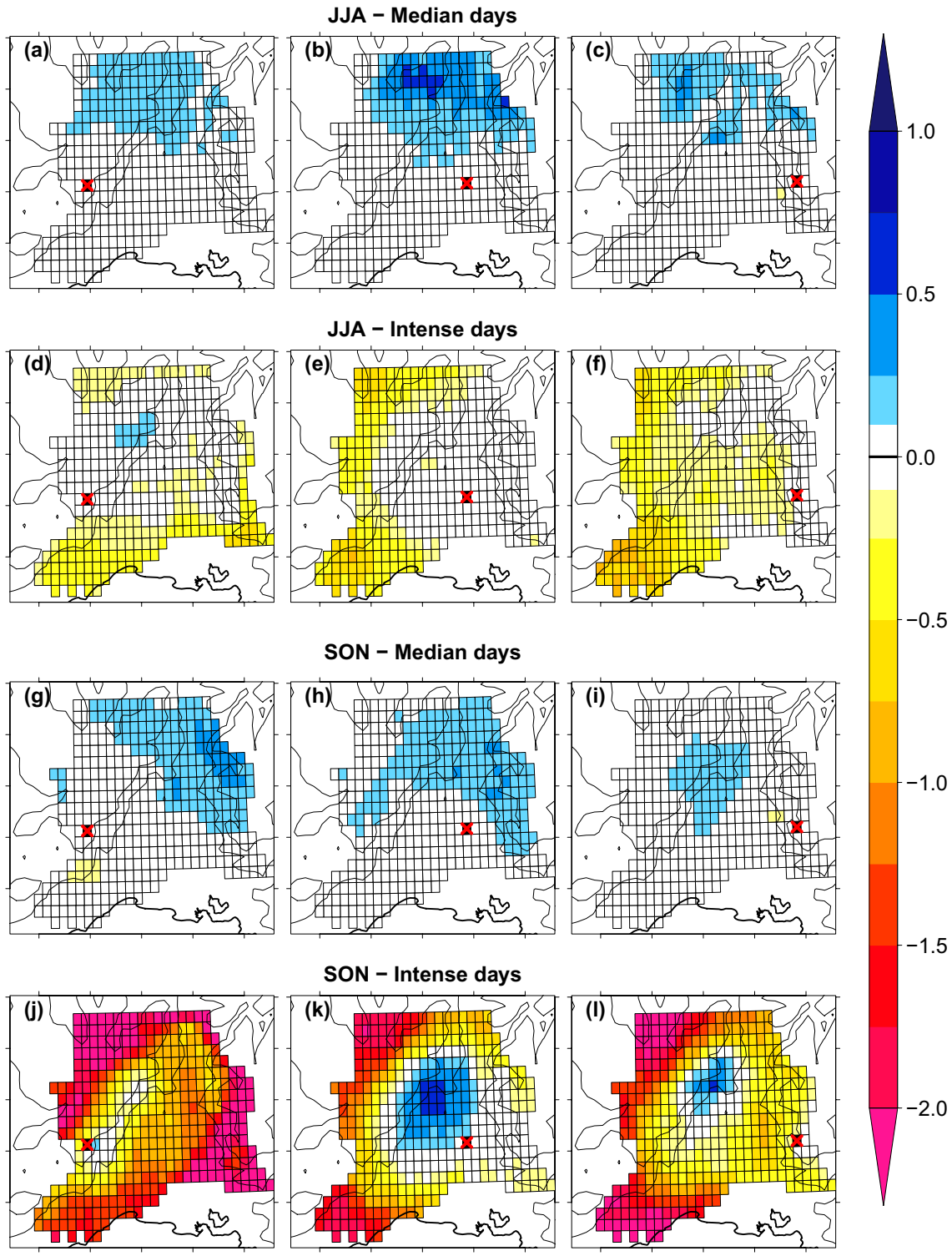

Fig. 15 Spatial repartition of the median value of precipitation intensity differences (in mm) with a reference *grid box* (*cross*) during summer median (**a–c**) and intense (**d–f**) days and autumn median (**g–i**) and intense (**j–l**) days). The reference *grid boxes* are the same as in Fig. 14. See Fig. 3 for more caption details

and autumn median and intense days. By and large, when a median daily intensity is observed in a grid box, the neighboring grid boxes tend to receive higher 3-h intensities (Fig. 15a–c, g–i). In contrast, if a day is intense in a given grid box, it is more likely to have lower 3-h intensities over the domain, except for some localized grid boxes (d–f, j–l).

This is consistent with the definition of median and intense days. In summer, around the reference grid boxes, the intensities are about the same in a rather large area, except in the Alps foothills intense days. During median days, the rainfall intensity structure at a larger distance seems to be driven by a south-north gradient. During the Cévennes intense days (Fig. 15d), higher intensities can be found in the north of the Cévennes mountain ridge, near Serre de la Croix de Bauzon.

In autumn median days, close to the reference grid boxes, the intensities are roughly the same in a large area. At a larger distance from the reference grid boxes, the intensities seem to be reinforced over the relief. In particular, during median days relatively to the Alp foothills, the rain intensity is larger over the north of the Cévennes. Besides, when a day is median with respect to the Cévennes region, the intensities are reinforced to the north-east, even though rain seldom occurs in both places simultaneously. Finally, during autumn intense days, the rainfall intensity structure close to the reference grid boxes is not prevailing. When the reference is in the south of the Cévennes, the same intensity is likely to occur over the all Cévennes mountain ridge. As the heavy quantiles are also similar, it denotes the homogeneity of the rain intensity over the Cévennes relief, pointing out the role of the relief in the generation of intense precipitation. The rain intensity structure is different when the reference grid box is taken in the plain or in the Alps foothill. In these two cases, it is noteworthy that the rain intensity is enhanced at the same location in both cases, that is near Serre de la Croix de Bauzon. Comparing the mean and the median of the intensity differences (not shown) indicates an enhancement even more important for heavier events. This is in agreement with the assumption of the blocking role of these mountains reported in Molinié et al. (2012) and simulated in Yates (2006). The intensity pattern shown here, mainly aloof from the reference grid boxes, may be associated with specific rainfall regimes rather than with the rain intensity structure inside a unique rain cell. A more detailed analysis of these rainfall regimes need to be carried out to determine their nature and their link with these intensity patterns. In conclusion, this analysis disclose the key influence of the relief on the rainfall structure and the differences between the Cévennes and the Alps in their influence.

7 Conclusion

This study describes a climatology of rainfall in Southeast France. The climatology relies on a database (named K-REF) of rainfall fields, with resolutions of 3 h and 0.1° in latitude and longitude, specifically designed to assess RCM-simulated rainfall. Kriging rainfall from hourly raingauge records from 1993 to 2013 has provided the rainfall fields of K-REF. K-REF is assessed relatively to the SAFRAN daily rainfall. The rainfall fields are smoother in K-REF than in SAFRAN but their patterns and magnitudes are in agreement.

Among the multiple facets of the rainfall climatology, this study shows in particular the influence of the relief and of the solar cycle in the triggering and the intensity of rain. The analysis of the diurnal cycles of rain occurrence and intensity especially illustrates that rainfall is preferentially triggered at the end of the afternoon, mainly during the most intense days. The variety of air mass characteristics flowing over the study region and their interactions with the relief may lead to various rainfall features. An important one relates to the Cévennes mountain ridge, characterized by high annual amounts of rainfall, about 1600 mm in average, which is almost three times greater than over the plain. Moreover, the ridge is also distinguished by high rain intensities both for 3 and 24-h accumulation periods, high rain occurrence and long lasting rainy events. It is worth noting that both high occurrence and high intensity of the 3-h rain combine during intense days in the Cévennes, pointing out the triggering and blocking roles of the relief on the precipitation. About 80 % of the 3-h periods are rainy during these intense days, and almost 40 % of them are all rainy. In addition, intense days are made of the highest of the 3-h intensities. Besides, the spatial structures of rain occurrence and intensity are also highly influenced by the Cévennes mountain range. When rain occurs in the Cévennes, the patterns of the average rain fields reflect the underlying topography while it is not the case over the rest of the domain, specifically the Alps foothills which are of comparable altitude.

Acknowledgments This work is part of the Med-CORDEX initiative (www.medcordex.eu) supported by the HYdrological cycle in The Mediterranean EXperiment (HyMeX) programme (www.hymex.org). This research has received funding from the French National Research Agency (ANR) project REMEMBER (contract ANR-12-SENV-001). The rainfall data were provided by Météo-France, in the framework of the OHM-CV observation service funded by CNRS/INSU and Université Grenoble Alpes/OSUG.

References

Alpert P (1986) Mesoscale indexing of the distribution of orographic precipitation over high mountains. J Clim Appl Meteorol 25(4):532–545

Alpert P, Shafir H (1989) Mesoγ-scale distribution of orographic precipitation: numerical study and comparison with precipitation derived from radar measurements. J Appl Meteorol 28(10):1105–1117

Bastin G, Lorent B, Duqué C, Gevers M (1984) Optimal estimation of the average areal rainfall and optimal selection of rain gauge locations. Water Resour Res 20(4):463–470. doi:10.1029/WR020i004p00463

Bastin S, Drobinski P, Dabas A, Delville P, Reitebuch O, Werner C (2005) Impact of the Rhône and Durance valleys on sea-breeze circulation in the Marseille area. Atmos Res 74(1):303–328. doi:10.1016/j.atmosres.2004.04.014

Berne A, Delrieu G, Boudevillain B (2009) Variability of the spatial structure of intense Mediterranean precipitation. Adv Water Resour 32(7):1031–1042

Biasutti M, Yuter SE, Burleyson CD, Sobel AH (2012) Very high resolution rainfall patterns measured by TRMM precipitation radar: seasonal and diurnal cycles. Clim Dyn 39(1–2):239–258. doi:10.1007/s00382-011-1146-6

Boé J, Terray L, Habets F, Martin E (2007) Statistical and dynamical downscaling of the Seine basin climate for hydro-meteorological studies. Int J Clim 27(12):1643–1655. doi:10.1002/joc.1602

Ceresetti D, Molinié G, Creutin JD (2010) Scaling properties of heavy rainfall at short duration: a regional analysis. Water Resour Res 46(9):W09,531. doi:10.1029/2009WR008603

Ceresetti D, Anquetin S, Molinié G, Leblois E, Creutin JD (2012) Multiscale evaluation of extreme rainfall event predictions using severity diagrams. Weather Forecast 27(1):174–188. doi:10.1175/WAF-D-11-00003.1

Chardon J, Hingray B, Favre AC, Autin P, Gailhard J, Zin I, Obled C (2014) Spatial similarity and transferability of analog dates for precipitation downscaling over France. J Clim 27(13):5056–5074. doi:10.1175/JCLI-D-13-00464.1

Chen CT, Knutson T (2008) On the verification and comparison of extreme rainfall indices from climate models. J Clim 21(7):1605–1621. doi:10.1175/2007JCLI1494.1

Chilès JP, Delfiner P (1999) Geostatistics. Modeling Spatial Uncertainty, Wiley-Interscience Publication Edition. Wiley Series in Probability and Statistics, Wiley, New York

Creutin JD, Obled C (1982) Objective analyses and mapping techniques for rainfall fields: an objective comparison. Water Resour Res 18(2):413–431. doi:10.1029/WR018i002p00413

Dai A (2006) Precipitation characteristics in eighteen coupled climate models. J Clim 19(18):4605–4630. doi:10.1175/JCLI3884.1

Dai A, Giorgi F, Trenberth KE (1999) Observed and model-simulated diurnal cycles of precipitation over the contiguous United States. J Geophys Res Atmos 104(D6):6377–6402. doi:10.1029/98JD02720

Dai A, Lin X, Hsu KL (2007) The frequency, intensity, and diurnal cycle of precipitation in surface and satellite observations over low- and mid-latitudes. Clim Dyn 29(7–8):727–744. doi:10.1007/s00382-007-0260-y

De Michele C, Kottegoda NT, Rosso R (2001) The derivation of areal reduction factor of storm rainfall from its scaling properties. Water Resour Res 37(12):3247–3252. doi:10.1029/2001WR000346

Delhomme JP (1978) Kriging in the hydrosciences. Adv Water Resour 1(5):251–266. doi:10.1016/0309-1708(78)90039-8

Delrieu G, Ducrocq V, Gaume E, Nicol J, Payrastre O, Yates E, Kirstetter PE, Andrieu H, Ayral PA, Bouvier C, Creutin JD, Livet M, Anquetin S, Lang M, Neppel L, Obled C, Parent-du-Châtelet J, Saulnier GM, Walpersdorf A, Wobrock W (2005) The catastrophic flash-flood event of 8–9 september 2002 in the Gard region, France: A first case study for the Cévennes-Vivarais mediterranean hydrometeorological observatory. J Hydrometeorol 6(1):34–52

Drobinski P, Bastin S, Dabas A, Delville P, Reitebuch O (2006) Variability of three-dimensional sea breeze structure in southern France: observations and evaluation of empirical scaling laws. Ann Geophys 24(7):1783–1799

Ducrocq V, Nuissier O, Ricard D, Lebeaupin C, Thouvenin T (2008) A numerical study of three catastrophic precipitating events over southern France. II: Mesoscale triggering and stationarity factors. Q J R Meteorol Soc 134(630):131–145. doi:10.1002/qj.199

Flato G, Marotzke J, Abiodun B, Braconnot P, Chou S, Collins W, Cox P, Driouech F, Emori S, Eyring V, Forest C, Gleckler P, Guilyardi E, Jakob C, Kattsov V, Reason C, Rummukainen M (2013) Evaluation of climate models. In: Climate Change 2013: The Physical Science Basis. Contribution of Working Group I to the Fifth Assessment Report of the Intergovernmental Panel on Climate Change, cambridge university press edn, Stocker, T.F., D. Qin, G.-K. Plattner, M. Tignor, S.K. Allen, J. Boschung, A. Nauels, Y. Xia, V. Bex and P.M. Midgley, Cambridge, United Kingdom and New York, NY, USA

Frei C, Schär C (1998) A precipitation climatology of the Alps from high-resolution rain-gauge observations. Int J Climatol 18(8):873–900

Fresnay S, Hally A, Garnaud C, Richard E, Lambert D (2012) Heavy precipitation events in the Mediterranean: sensitivity to cloud physics parameterisation uncertainties. Nat Hazards Earth Syst Sci 12(8):2671–2688. doi:10.5194/nhess-12-2671-2012

Giorgi F (2006) Climate change hot-spots. Geophys Res Lett 33(L08):707. doi:10.1029/2006GL025734

Giorgi F, Lionello P (2008) Climate change projections for the Mediterranean region. Glob Planet Change 63:90–104. doi:10.1016/j.gloplacha.2007.09.005

Giorgi F, Jones C, Asrar GR (2009) Addressing climate information needs at the regional level: the CORDEX framework. World Meteorol Organ (WMO) Bull 58(3):175

Giorgi F, Im ES, Coppola E, Diffenbaugh NS, Gao XJ, Mariotti L, Shi Y (2011) Higher Hydroclimatic Intensity with Global Warming. J Clim 24(20):5309–5324. doi:10.1175/2011JCLI3979.1

Godart A, Anquetin S, Leblois E (2009) Rainfall regimes associated with banded convection in the Cévennes-Vivarais area. Meteorol Atmos Phys 103(1–4):25–34. doi:10.1007/s00703-008-0326-3

Godart A, Leblois E, Anquetin S, Freychet N (2010) Analysis of the relationship between banded orographic convection and atmospheric properties using factorial discriminant analysis and neural networks. J Appl Meteorol Climatol 49(4):646–663. doi:10.1175/2009JAMC2217.1

Godart A, Anquetin S, Leblois E, Creutin JD (2011) The contribution of orographically driven banded precipitation to the rainfall climatology of a Mediterranean region. J Appl Meteorol Climatol 50(11):2235–2246. doi:10.1175/JAMC-D-10-05016.1

Haylock MR, Hofstra N, Klein Tank AMG, Klok EJ, Jones PD, New M (2008) A european daily high-resolution gridded data set of surface temperature and precipitation for 1950–2006. J Geophys Res Atmos 113(D20):119. doi:10.1029/2008JD010201

Hewitson BC, Crane RG (1996) Climate downscaling: techniques and application. Clim Res 07(2):85–95. doi:10.3354/cr007085

Hill CM, Fitzpatrick PJ, Corbin JH, Lau YH, Bhate SK (2010) Summertime precipitation regimes associated with the sea breeze and land breeze in Southern Mississippi and Eastern Louisiana. Weather Forecast 25(6):1755–1779. doi:10.1175/2010WAF2222340.1

Huffman GJ, Adler RF, Morrissey MM, Bolvin DT, Curtis S, Joyce R, McGavock B, Susskind J (2001) Global precipitation at one-degree daily resolution from multisatellite observations. J Hydrometeorol 2(1):36–50

Johnson GL, Hanson CL (1995) Topographic and atmospheric influences on precipitation variability over a mountainous watershed. J Appl Meteorol 34(1):68–87. doi:10.1175/1520-0450-34.1.68

Koutsoyiannis D (1997) Statistical hydrology. Dep Water Resour Hydraul and Maritime Eng Natl Tech Univ of Athens, Athens, Greece

Lebel T, Bastin G, Obled C, Creutin JD (1987) On the accuracy of areal rainfall estimation: a case study. Water Resour Res 23(11):2123–2134. doi:10.1029/WR023i011p02123

Leblois E, Creutin JD (2013) Space-time simulation of intermittent rainfall with prescribed advection field: adaptation of the turning

band method: Simulation of Rainfall with Advection Field. Water Resour Res 49(6):3375–3387. doi:10.1002/wrcr.20190

Lepioufle JM, Leblois E, Creutin JD (2012) Variography of rainfall accumulation in presence of advection. J Hydrol 464–465:494–504. doi:10.1016/j.jhydrol.2012.07.041

Mandapaka PV, Germann U, Panziera L (2013) Diurnal cycle of precipitation over complex Alpine orography: inferences from high-resolution radar observations. Q J R Meteorol Soc 139(673):1025–1046. doi:10.1002/qj.2013

Maraun D, Wetterhall F, Ireson AM, Chandler RE, Kendon EJ, Widmann M, Brienen S, Rust HW, Sauter T, Themel M, Venema VKC, Chun KP, Goodess CM, Jones RG, Onof C, Vrac M, Thiele-Eich I (2010) Precipitation downscaling under climate change: Recent developments to bridge the gap between dynamical models and the end user. Reviews of Geophysics 48(3):RG3003, doi:10.1029/2009RG000314

Mariotti A, Pan Y, Zeng N, Alessandri A (2015) Long-term climate change in the Mediterranean region in the midst of decadal variability. Clim Dyn 44(5–6):1437–1456. doi:10.1007/s00382-015-2487-3

Mearns LO, Bogardi I, Giorgi F, Matyasovszky I, Palecki M (1999) Comparison of climate change scenarios generated from regional climate model experiments and statistical downscaling. J Geophys Res Atmos 104(D6):6603–6621. doi:10.1029/1998JD200042

Michaud J, Auvine BA, Penalba OC (1995) Spatial and elevational variations of summer rainfall in the southwestern United States. J Appl Meteorol 34(12):2689–2703

Miniscloux F, Creutin JD, Anquetin S (2001) Geostatistical analysis of orographic rainbands. J Appl Meteorol 40(11):1835–1854

Mitchell TD, Jones PD (2005) An improved method of constructing a database of monthly climate observations and associated high-resolution grids. Int J Climatol 25(6):693–712. doi:10.1002/joc.1181

Molinié G, Ceresetti D, Anquetin S, Creutin JD, Boudevillain B (2012) Rainfall regime of a mountainous mediterranean region: statistical analysis at short time steps. J Appl Meteorol Climatol 51(3):429–448. doi:10.1175/2011JAMC2691.1

Nesbitt SW, Zipser EJ (2003) The diurnal cycle of rainfall and convective intensity according to three years of TRMM measurements. J Clim 16(10):1456–1475

Nikulin G, Jones C, Giorgi F, Asrar G, Büchner M, Cerezo-Mota R, Christensen OB, Déqué M, Fernandez J, Hänsler A, van Meijgaard E, Samuelsson P, Sylla MB, Sushama L (2012) Precipitation climatology in an ensemble of CORDEX-Africa regional climate simulations. J Clim 25(18):6057–6078. doi:10.1175/JCLI-D-11-00375.1

Nuissier O, Ducrocq V, Ricard D, Lebeaupin C, Anquetin S (2008) A numerical study of three catastrophic precipitating events over southern France. I: Numerical framework and synoptic ingredients. Q J R Meteorol Soc 134(630):111–130. doi:10.1002/qj.200

Oki T, Musiake K (1994) Seasonal change of the diurnal cycle of precipitation over Japan and Malaysia. J Appl Meteorol 33(12):1445–1463

Pielke RA (1974) A three-dimensional numerical model of the sea breezes over South Florida. Mon Weather Rev 102(2):115–139

Quintana-Seguí P, Le Moigne P, Durand Y, Martin E, Habets F, Baillon M, Canellas C, Franchisteguy L, Morel S (2008) Analysis of near-surface atmospheric variables: validation of the SAFRAN analysis over france. J Appl Meteorol Climatol 47(1):92–107. doi:10.1175/2007JAMC1636.1

Quintana-Seguí P, Ribes A, Martin E, Habets F, Boé J (2010) Comparison of three downscaling methods in simulating the impact of climate change on the hydrology of Mediterranean basins. J Hydrol 383(1–2):111–124. doi:10.1016/j.jhydrol.2009.09.050

Quintana Seguí P (2008) Simulation hydrologique en région méditerranéenne avec SAFRAN-ISBA-MODCOU. Amélioration de la physique et évaluation des risques dans le cadre du changement climatique. PhD thesis, Université Paul Sabatier, Toulouse, France

Reichler T, Kim J (2008) How well do coupled models simulate today's climate? Bull Am Meteorol Soc 89(3):303–311. doi:10.1175/BAMS-89-3-303

Ricard D (2002) Initialisation et assimilation de données à méso-échelle pour la prévision à haute résolution des pluies intenses de la région Cévennes-Vivarais. PhD thesis, Université Paul Sabatier-Toulouse III, France

Ruin I, Creutin JD, Anquetin S, Lutoff C (2008) Human exposure to flash floods-Relation between flood parameters and human vulnerability during a storm of September 2002 in southern France. J Hydrol 361(1–2):199–213. doi:10.1016/j.jhydrol.2008.07.044

Ruti PM, Somot S, Giorgi F, Dubois C, Flaounas E, Obermann A, Dell'Aquila A, Pisacane G, Harzallah A, Lombardi E, Ahrens B, Akhtar N, Alias A, Arsouze T, Aznar R, Bastin S, Bartholy J, Béranger K, Beuvier J, Bouffies-Cloché S, Brauch J, Cabos W, Calmanti S, Calvet JC, Carillo A, Conte D, Coppola E, Djurdjevic V, Drobinski P, Elizalde-Arellano A, Gaertner M, Galàn P, Gallardo C, Gualdi S, Goncalves M, Jorba O, Jordà G, L'Heveder B, Lebeaupin-Brossier C, Li L, Liguori G, Lionello P, Macià S D, Nabat P, Onol B, Raikovic B, Ramage K, Sevault F, Sannino G, Struglia M, Sanna A, Torma C, Vervatis V (2015) MED-CORDEX initiative for Mediterranean climate studies. Bull Am Meteorol Soc. doi:10.1175/BAMS-D-14-00176.1

Sénési S, Bougeault P, Chèze JL, Cosentino P, Thepenier RM (1996) The Vaison-La-Romaine Flash flood: mesoscale analysis and predictability issues. Weather Forecast 11(4):417–442

Skelly WC, Henderson-Sellers A (1996) Grid box or grid point: what type of data do GCMs deliver to climate impact researchers? Int J Climatol 16(10):1079–1086

Vidal JP, Martin E, Franchistéguy L, Baillon M, Soubeyroux JM (2010) A 50-year high-resolution atmospheric reanalysis over France with the Safran system. Int J Climatol 30(11):1627–1644. doi:10.1002/joc.2003

Vié B, Molinié G, Nuissier O, Vincendon B, Ducrocq V, Bouttier F, Richard E (2012) Hydro-meteorological evaluation of a convection-permitting ensemble prediction system for Mediterranean heavy precipitating events. Nat Hazards Earth Syst Sci 12(8):2631–2645. doi:10.5194/nhess-12-2631-2012

Xie P, Arkin PA (1997) Global precipitation: a 17-year monthly analysis based on gauge observations, satellite estimates, and numerical model outputs. Bull Am Meteorol Soc 78(11):2539–2558

Yates E (2006) Convection en région Cévennes-Vivarais: Etude de données pluviométriques, simulations numériques et validation multi-échelles. PhD thesis, Institut National Polytechnique de Grenoble, France

Yates E, Anquetin S, Ducrocq V, Creutin JD, Ricard D, Chancibault K (2006) Point and areal validation of forecast precipitation fields. Meteorol Appl 13(01):1–20. doi:10.1017/S1350482705001921

Zepeda-Arce J, Foufoula-Georgiou E, Droegemeier KK (2000) Space-time rainfall organization and its role in validating quantitative precipitation forecasts. J Geophys Res Atmos 105(D8):10,129–10,146. doi:10.1029/1999JD901087